Journal of Optical Technology

Acousto-optic spatial frequency filter operating in the intermediate region of acousto-optic interaction

V. M. Kotov,[1,2] S. V. Averin,[1] M. V. Karachevzeva,[1] and N. G. Yaremenko[1]

[1]Kotel'nikov Institute of Radioengineering and Electronics, Russian Academy of Sciences, Fryazino, Russia
[2]e-mail: vmk6054@mail.ru

Received 6 October 2021; Opticheskiĭ Zhurnal **89**, 54–62 (January 2022)

The characteristics of an acousto-optic spatial frequency filter designed for processing of two-dimensional images and operation in the intermediate region of acousto-optic diffraction are investigated. The advantage of such filters over filters operating in a Bragg regime is the possibility of operation at significantly lower acoustic frequencies, which allows the passband of spatial frequencies to be increased and the limiting resolution to be decreased. Transfer functions of diffraction orders are obtained. The use of the first diffraction order is demonstrated to allow selection of the two-dimensional image contour. The two-dimensional image edge enhancement of the image transmitted by optical emission at a wavelength of 0.63×10^{-4} cm is experimentally demonstrated using a TeO_2 spatial filter operating at a frequency of 15 MHz.

OCIS codes: (070.1060) Acousto-optical signal processing, (070.2615) Frequency filtering, (070.6110) Spatial filtering.

https://doi.org/10.1364/JOT.89.000038

1. INTRODUCTION

Optical Fourier methods are ubiquitous in image processing owing to the simplicity of their practical implementation and extremely high operation speed [1–3]. A spatial filter is a basic element of Fourier processing that essentially determines the properties of the processed images. Controllable acousto-optic (AO) cells with a relatively high operation speed, low control power, broad band of acoustic frequencies, reliability, and design simplicity are often used as filters [4,5].

AO elements have become seamlessly integrated into the systems for optical image processing because they allow the amplitude and phase structure of the optical field carrying the image to be significantly changed [6,7]. AO elements operating in the Bragg diffraction mode, when the Klein–Cook parameter $Q \approx \mathbf{q}^2 L/\mathbf{K}$ significantly exceeds unity, are most often used in practice [8,9], where $\mathbf{q}$ and $\mathbf{K}$ are the wave vectors of sound and light, respectively, and L is the length of AO interaction.

Multiple variants of AO Bragg diffraction were proposed and investigated for two-dimensional image processing. Variants using tangential and collinear geometries of AO interaction [4–7,10] appeared to be the most efficient among the variants of diffraction into a single Bragg order. The application of multiple diffraction modes opens wider possibilities [11–16]. For example, the filtering properties of the 0th diffraction order in the process of light diffraction into the +1st and −1st orders were investigated in [11]. It is commonly known that this mode [8] is characterized by the minimum consumption of acoustic power. The possibility to form a two-dimensional filter in two diffraction orders simultaneously in the course of triple AO interaction was demonstrated in [12]. Filtering properties of double diffraction in conjunction with an external polarizer were considered in [13]. The contour formation was demonstrated to be possible at different levels of acoustic power but at different polarizer positions. Contour formation in the course of polarization-independent diffraction was investigated in [14]. This variant, essentially, allows the use of a single AO cell instead of two. Two-dimensional properties of Bragg diffraction orders formed as a result of the combination of beams with similar or different polarizations were considered in general in [15]. The formation of an optical field for two-dimensional image processing based on "common" Bragg diffraction but with minimum contribution of diffraction into the additional side order was investigated in [16]. A 20% contribution of the side order into the total field ensured the selection of the two-dimensional contour.

In practice, Bragg diffraction regimes are realized by an accurate setting of diffraction to the Bragg resonance followed by selection of the optimal area of the optical field allowing two-dimensional image processing through scanning of the AO cell across the optical radiation combined with variation in acoustic power.

In the case of transition to the intermediate diffraction regime, the resonant properties of AO interaction weaken and changes in sound frequency and angular orientation of the AO cell are possible. However, in this case, the portion of the optical

radiation in the "operational" diffraction order used for the two-dimensional processing decreases. In this regime, all radiation cannot be concentrated in a single diffraction order. In terms of the properties of the spatial filter, the intermediate diffraction regime is more advantageous than the Bragg regime because it allows the sound frequency and AO interaction length to be significantly reduced, thus ensuring the increase in the passband of spatial frequencies and reduction in limiting image resolution [17]. In other words, identification of smaller image features becomes possible.

Notably, the diffraction in the intermediate region was investigated by many researchers [8,18–24]. We investigated, for the first time to our knowledge, the filtering properties of such diffraction in application to the two-dimensional image processing. Parameters that determine the properties of diffracted radiation distribution significantly depend on the AO interaction model, i.e., curvature of the surfaces of the crystal wave vectors, type of AO diffraction, and ellipticity of the optical rays. All mentioned factors were considered in this study. Two-dimensional distributions of optical fields in each diffraction order were obtained. An area ensuring the selection of a two-dimensional image contour was found in the first diffraction order. The presence of such an area was confirmed experimentally.

2. THEORY

In the intermediate regime of AO diffraction, the radiation diffracts into several diffraction orders besides the first principal order. We assume that the −1st and +2nd orders are the additional diffraction orders. Events of diffraction into higher orders are considered insignificant and are disregarded. All considered diffraction events are shown in the vector diagram in Fig. 1. The AO interaction is assumed to occur in a uniaxial gyrotropic crystal such as TeO_2 crystal. In a strict consideration,

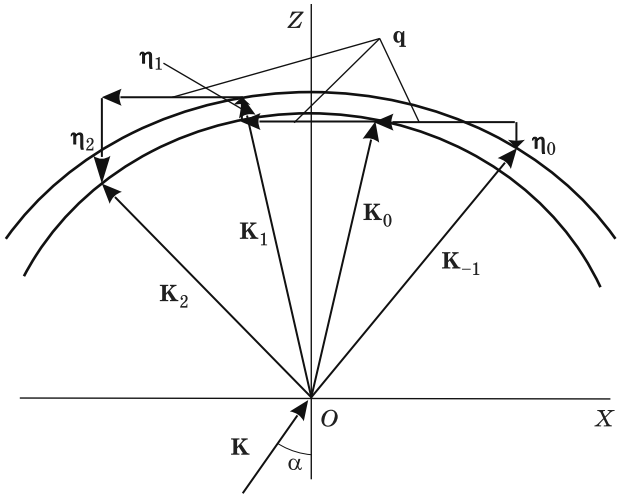

Fig. 1. Vector diagram of the AO diffraction into four orders. **K** is the wave vector of the emission incident on the optical facet *OX* of the crystal at angle α; $\mathbf{K}_0$ is the wave vector of the incident radiation inside the crystal; $\mathbf{K}_{-1}$, $\mathbf{K}_1$, and $\mathbf{K}_2$ are the wave vectors of the −1st, +1st, and +2nd diffraction orders, respectively; **q** is the sound wave vector; η_0, η_1, and η_2 are the vectors of Bragg synchronism detunings; and *OZ* is the optical axis of the crystal.

the vector diagram is three-dimensional [25]. We present a two-dimensional diagram even though its three-dimensionality is implied. The initial optical radiation with a wave vector **K** is incident at an angle α on the optical facet *OX* of the crystal oriented orthogonally to its optical axis *OZ*. The wave vector of incident radiation inside the crystal is represented by the vector $\mathbf{K}_0$. Diffraction of light occurs on the acoustic wave with a wave vector **q**. All diffraction events are anisotropic. Radiation diffracting into the first order is represented with a wave vector $\mathbf{K}_1$. Moreover, besides the first order, diffraction also occurs into the −1st and +2nd diffraction orders with wave vectors $\mathbf{K}_{-1}$ and $\mathbf{K}_2$, respectively. Phase detuning vectors of the diffraction orders are denoted as η_0, η_1, and η_2. The amplitudes of the diffracted rays are searched based on the coupled-wave theory [8], according to which the diffraction presented in Fig. 1 is described by the following system of differential equations:

$$\begin{aligned}
\frac{dC_0}{dz} &= -A_1 C_{-1}\exp(-i\eta_0 z) - A_2 C_1 \exp(-i\eta_1 z),\\
\frac{dC_{-1}}{dz} &= A_1 C_0 \exp(i\eta_0 z),\\
\frac{dC_1}{dz} &= A_2 C_0 \exp(i\eta_1 z) - A_3 C_2 \exp(-i\eta_2 z),\\
\frac{dC_2}{dz} &= A_3 C_1 \exp(i\eta_2 z),
\end{aligned} \tag{1}$$

where C_0, C_{-1}, C_1, and C_2 are the amplitudes of rays $\mathbf{K}_0$, $\mathbf{K}_{-1}$, $\mathbf{K}_1$, and $\mathbf{K}_2$, respectively; z is the coordinate along which the AO interaction occurs; η_0, η_1, and η_2 are the phase detuning vectors;

$$A_1 = \frac{v}{4} f_{0,-1},\ A_2 = \frac{v}{4} f_{0,1},\ A_3 = \frac{v}{4} f_{2,1}, \tag{2}$$

where $f_{0,-1}$, $f_{0,1}$, and $f_{2,1}$ are the coefficients considering the ellipticity of the interacting rays [13]:

$$\begin{aligned}
f_{0,-1} &= (1+\rho_0\rho_{-1})\left[\left(1+\rho_0^2\right)\left(1+\rho_{-1}^2\right)\right]^{-0.5},\\
f_{0,1} &= (1+\rho_0\rho_1)\left[\left(1+\rho_0^2\right)\left(1+\rho_1^2\right)\right]^{-0.5},\\
f_{2,1} &= (1+\rho_2\rho_1)\left[\left(1+\rho_2^2\right)\left(1+\rho_1^2\right)\right]^{-0.5},
\end{aligned}$$

where ρ_k is the ellipticity of the kth ray ($k = -1, 0, 1, 2$) equal to

$$\rho_k = 0.5 G_{33}^{-1}\left(\sqrt{T^2 + 4G_{33}^2} - T\right). \tag{3}$$

The parameter G_{33} in Eq. (3) is the component of the gyration pseudotensor:

$$T = \frac{\tan^2\theta\left(n_e^2 - n_0^2\right)}{n_0^2 n_e^2(1+\tan^2\theta)},$$

where θ is the angle between the light wave vector and optical axis of the crystal, and n_o and n_e are the principal refractive indices of the crystal. The coefficient v in Eq. (2) is the Raman–Nath parameter considering the AO properties of the medium and acoustic power:

$$v = \frac{2\pi}{\lambda}\sqrt{\frac{M_2 P_a}{2LH}},$$

where λ is the radiation wavelength, M_2 is the coefficient of material AO quality, P_a is the acoustic power, L is the length of AO interaction, and H is the height of the acoustic column. Therefore, A_1, A_2, and A_3 in Eq. (1) depend on the acoustic power and ray ellipticity.

According to the method proposed in [26], a particular solution to system (1) can be found in the following form:

$$C_0 = a\exp(i\alpha z),\ C_{-1} = b\exp(i\beta z),$$
$$C_1 = c\exp(i\gamma z),\ C_2 = d\exp(i\delta z), \tag{4}$$

where a, b, c, d, α, β, γ, and δ are the parameters independent of z, which should be determined. After substitution of Eqs. (4) into system (1), we obtain the following system of equations:

$$\begin{aligned} ia\alpha\exp(i\alpha z) &= -A_1 b\exp[i(\beta-\eta_0)z] \\ &\quad - A_2 c\exp[i(\gamma-\eta_1)z], \\ ib\beta\exp(i\beta z) &= A_1 a\exp[i(\alpha+\eta_0)z], \\ ic\gamma\exp(i\gamma z) &= A_2 a\exp[i(\alpha+\eta_1)z] \\ &\quad - A_3 d\exp[i(\delta-\eta_2)z], \\ id\delta\exp(i\delta z) &= A_3 c\exp[i(\gamma+\eta_2)z]. \end{aligned} \tag{5}$$

For each of the equations of system (5) to be valid at any z, the coefficients in the exponents of each equation should be equal:

$$\alpha = \beta-\eta_0 = \gamma-\eta_1,\ \beta = \alpha+\eta_0,$$
$$\gamma = \alpha+\eta_1 = \delta-\eta_2,\ \delta = \gamma+\eta_2. \tag{6}$$

We express β, γ, and δ through α:

$$\beta = \alpha+\eta_0,\ \gamma = \alpha+\eta_1,\ \delta = \alpha+\eta_0+\eta_1. \tag{7}$$

If conditions (6) are fulfilled, system of equations (5) is simplified and has the following form:

$$\begin{aligned} ia\alpha &= -A_1 b - A_2 c, \\ ib\beta &= A_1 a, \\ ic\gamma &= A_2 a - A_3 d, \\ id\delta &= A_3 c. \end{aligned} \tag{8}$$

The equations of system (8) can be expressed as a system of homogeneous equations with unknown a, b, c, and d. Considering Eq. (7), the principal determinant of system (8) is equal to

$$D = \begin{vmatrix} i\alpha & A_1 & A_2 & 0 \\ A_1 & -i(\alpha+\eta_0) & 0 & 0 \\ A_2 & 0 & -i(\alpha+\eta_1) & -A_3 \\ 0 & 0 & A_3 & -i(\alpha+\eta_1+\eta_2) \end{vmatrix}. \tag{9}$$

System (8) has a nontrivial solution only when $D = 0$. By expanding D, we obtain a fourth-order secular equation with respect to α:

$$\alpha^4 + B_3\alpha^3 + B_2\alpha^2 + B_1\alpha + B_0 = 0, \tag{10}$$

where

$$\begin{aligned} B_3 &= \eta_0 + 2\eta_1 + \eta_2, \\ B_2 &= \eta_0(\eta_1+\eta_2) \\ &\quad + \eta_1(\eta_0+\eta_1+\eta_2) - (A_1^2 + A_2^2 + A_3^2), \\ B_1 &= \eta_0\eta_1(\eta_1+\eta_2) - A_1^2(2\eta_1+\eta_2) \\ &\quad - A_2^2(\eta_0+\eta_1+\eta_2) - A_3^2\eta_0, \\ B_0 &= A_1^2A_3^2 - A_1^2\eta_1(\eta_1+\eta_2) - A_2^2\eta_0(\eta_1+\eta_2). \end{aligned} \tag{11}$$

We express coefficients b, c, and d through coefficient a according to Eqs. (8):

$$b = -\frac{iA_1 a}{\alpha+\eta_0},\ c = -\frac{i}{A_2}\left[\alpha - \frac{A_1^2}{(\alpha+\eta_0)}\right]a,$$
$$d = -\frac{A_3}{A_2}\left[\alpha - \frac{A_1^2}{(\alpha+\eta_0)}\right]\frac{a}{\alpha+\eta_1+\eta_2}. \tag{12}$$

Considering Eq. (7), the general solution for the amplitudes is

$$\begin{aligned} C_0 &= \sum_{k=1}^{4} a_k\exp(i\alpha_k z), \\ C_{-1} &= \sum_{k=1}^{4} b_k\exp[i(\alpha_k+\eta_0)z], \\ C_1 &= \sum_{k=1}^{4} c_k\exp[i(\alpha_k+\eta_1)z], \\ C_2 &= \sum_{k=1}^{4} d_k\exp[i(\alpha_k+\eta_1+\eta_2)z], \end{aligned} \tag{13}$$

where α_k are the roots of Eq. (10) and coefficients b_k, c_k, and d_k are associated with a_k by Eqs. (12). k has values of 1, 2, 3, and 4.

Under the boundary conditions,

$$\sum_{k=1}^{4} a_k = 1,$$
$$\sum_{k=1}^{4} b_k = \sum_{k=1}^{4} c_k = \sum_{k=1}^{4} d_k = 0 \quad \text{when } z = 0, \tag{14}$$

Eqs. (13) transform into a system of linear inhomogeneous equations with respect to a_1, a_2, a_3, and a_4:

$$a_1 + a_2 + a_3 + a_4 = 1,$$

$$\frac{a_1}{\alpha_1 + \eta_0} + \frac{a_2}{\alpha_2 + \eta_0} + \frac{a_3}{\alpha_3 + \eta_0} + \frac{a_4}{\alpha_4 + \eta_0} = 0,$$

$$\left(\alpha_1 - \frac{A_1^2}{\alpha_1 + \eta_0}\right) a_1 + \left(\alpha_2 - \frac{A_1^2}{\alpha_2 + \eta_0}\right) a_2$$

$$+ \left(\alpha_3 - \frac{A_1^2}{\alpha_3 + \eta_0}\right) a_3 + \left(\alpha_4 - \frac{A_1^2}{\alpha_4 + \eta_0}\right) a_4 = 0,$$

$$\left(\alpha_1 - \frac{A_1^2}{\alpha_1 + \eta_0}\right) \frac{a_1}{\alpha_1 + \eta_1 + \eta_2} + \cdots$$

$$+ \left(\alpha_4 - \frac{A_1^2}{\alpha_4 + \eta_0}\right) \frac{a_4}{\alpha_4 + \eta_1 + \eta_2} = 0. \quad (15)$$

By solving system of equations (15), we obtain coefficients a_k and identify amplitudes C_0, C_{-1}, C_1, and C_2 using Eqs. (13). Finally, we obtain

$$C_0 = a_1 \exp(i\alpha_1 L) + a_2 \exp(i\alpha_2 L) + a_3 \exp(i\alpha_3 L) + a_4 \exp(i\alpha_4 L),$$

$$C_{-1} = b_1 \exp[i(\alpha_1 + \eta_0)L] + b_2 \exp[i(\alpha_2 + \eta_0)L] + b_3 \exp[i(\alpha_3 + \eta_0)L] + b_4 \exp[i(\alpha_4 + \eta_0)L],$$

$$C_1 = c_1 \exp[i(\alpha_1 + \eta_1)L] + c_2 \exp[i(\alpha_2 + \eta_1)L] + c_3 \exp[i(\alpha_3 + \eta_1)L] + c_4 \exp[i(\alpha_4 + \eta_1)L],$$

$$C_2 = d_1 \exp[i(\alpha_1 + \eta_1 + \eta_2)L] + d_2 \exp[i(\alpha_2 + \eta_1 + \eta_2)L] + d_3 \exp[i(\alpha_3 + \eta_1 + \eta_2)L] + d_4 \exp[i(\alpha_4 + \eta_1 + \eta_2)L]. \quad (16)$$

The amplitudes depend on the values of the synchronism detuning η_0, η_1, and η_2 and parameters A_1, A_2, and A_3, which, in turn, depend on the AO properties of the medium and sound power.

The two-dimensionality of the optical field distribution in every diffraction order is determined by the two-dimensionality of the synchronism detunings η_0, η_1, and η_2 present in the expressions for the amplitudes [Eqs. (16)]. The search for the distribution of the detuning values is a separate task that depends on the chosen model for the surfaces of crystal wave vectors. To find η_0, η_1, and η_2, we use a model where the refractive indices of a uniaxial gyrotropic crystal are determined from the following equations [27]:

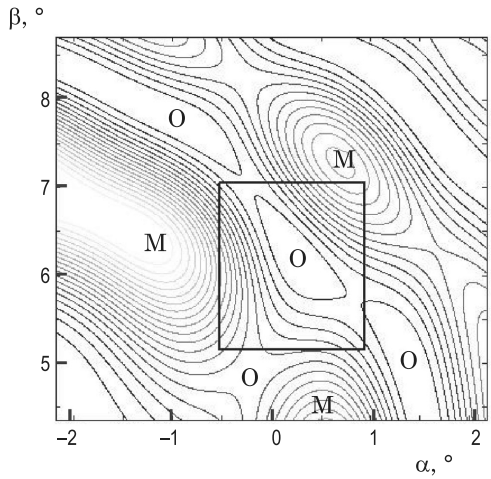

Fig. 2. Distribution $C_1 \times C_1^*$ of the 1st diffraction order under the variation of angles α and β. α is the angle between wave vector **K** of the radiation incident on the crystal and the OZ axis in the diffraction plane, while β is the angle between vector **K** and the diffraction plane. M and O are the maxima and minima of the distribution, respectively.

$$n_{1,2}^2 = 1 + \tan^2\theta \Big/ \left(\frac{1}{n_0^2} + \frac{\tan^2\theta}{2}\left(\frac{1}{n_0^2} + \frac{1}{n_e^2}\right) \pm \frac{1}{2}\sqrt{\tan^4\theta\left(\frac{1}{n_0^2} - \frac{1}{n_e^2}\right) + 4G_{33}^2}\right), \quad (17)$$

where θ, n_o, n_e, and G_{33} are the same parameters as in Eq. (3). The two-dimensionality of the processed image is described by angles α and β of the tilt of vector **K**, where α is the angle between **K** and the OZ axis in the diffraction plane and β is the angle between vector **K** and the diffraction plane. Only angle α is shown in Fig. 1. In the calculations, angle θ was expressed through angles α and β.

The calculations were performed using the following values of the parameters in Eqs. (1)–(17) [28,29]:

$$\lambda = 0.63 \times 10^{-4}\ \text{cm},\ n_o = 2.26,\ n_e = 2.41,$$

$$G_{33} = 2.62 \times 10^{-5},\ L = H = 0.2\ \text{cm},$$

$$M_2 = 1200 \times 10^{-18}\ \text{s}^3/\text{g},\ V = 0.617 \times 10^5\ \text{cm/s}.$$

The acoustic power and sound frequency were $P_a = 0.1$ W and $f = 15$ MHz, respectively (L, H, and f correspond to the experiment conditions). For these parameters, $Q \approx 2.07$. By calculating the amplitudes of diffraction maxima C_k, we can determine the intensity distributions $C_k \times C_k^*$, which are real values and represent the behavior of the transfer functions. The filtering properties of the +1st diffraction order were investigated in our experiments. The angular distribution of $C_1 \times C_1^*$ under the variation of angles α and β in the vicinity of the area ensuring the selection of the two-dimensional contour is shown in Fig. 2. The angular size of the distribution is approximately $4° \times 4°$. The distribution is strongly nonuniform. It comprises an assembly of maxima and minima with arbitrary mutual orientation. Distribution maxima and minima are denoted as

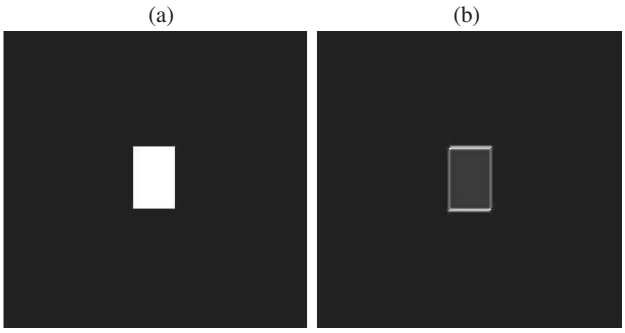

Fig. 3. Images (a) before and (b) after the FFT processing.

"M" and "O," respectively. An area ensuring the image differentiation is indicated in the distribution. The peculiarity of the indicated area is that it is located in a "valley" between three maxima. According to calculations, this area allows selection of a two-dimensional contour. A result of fast Fourier transform (FFT) processing of the image in the form of a rectangle with a distribution shown in Fig. 2 acting as a transfer function is shown in Fig. 3. Images before and after processing are shown in Figs. 3(a) and 3(b), respectively. Figure 3(b) is a well-defined two-dimensional contour of Fig. 3(a). In other words, the obtained transfer function acts as a two-dimensional spatial filter, which allows selection of the image contour.

3. EXPERIMENT AND DISCUSSION OF EXPERIMENTAL RESULTS

An experiment was carried out according to the optical scheme for Fourier processing (Fig. 4), which is described in detail in [16]. A He–Ne laser emitting at a wavelength of 0.63×10^{-4} cm acted as a radiation source. The AO cell acting as a spatial filter was fabricated from a TeO_2 monocrystal, in which the optical radiation diffracted on the slow acoustic wave with a frequency of 15 MHz. A hole in the form of a square with a side size of 0.3 mm acted as an input image. When the electric signal was applied to the AO cell, five images in the −1st, 0th, +1st, +2nd, and +3rd diffraction orders were observed on the output screen. The image intensity in the +3rd diffraction order did not exceed 2% of the incident radiation intensity. We investigated the contour formation in the +1st order. To this end, we attained the situation where a two-dimensional image contour was formed in the +1st order by angular adjustment of the AO cell, translation of the cell along the vertical axis, and tuning of the sound power. At the same time, the contour did not appear in other orders. Notably, a slight angular adjustment of the AO cell weakly affected the change in the effectiveness of the +1st order, which indicated the absence of sharp Bragg resonance. Figure 5 shows photographs of an image obtained in the 0th Bragg order in the absence of voltage applied to the transducer [Fig. 5(a)] and in the +1st order when a voltage of 7.05 V was applied to the transducer [Fig. 5(b)]. A well-defined two-dimensional contour is observed in the latter figure. In other words, the possibility to obtain a two-dimensional contour of an optical image using an AO spatial filter operating in an intermediate region of AO diffraction was experimentally confirmed.

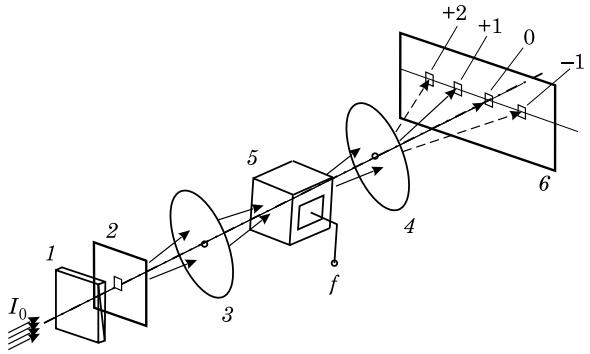

Fig. 4. Optical scheme of the experimental setup. I_0—incident optical radiation; *1*—quarter-wave plate; *2*—screen that forms the input image; *3*, *4*—lenses that perform the Fourier processing of the image; *5*—AO filter; *f*—signal fed to the filter; *6*—screen at which the result of Fourier processing is observed; −1, 0, +1, +2—images of the −1st, 0th, +1st, and +2nd diffraction orders.

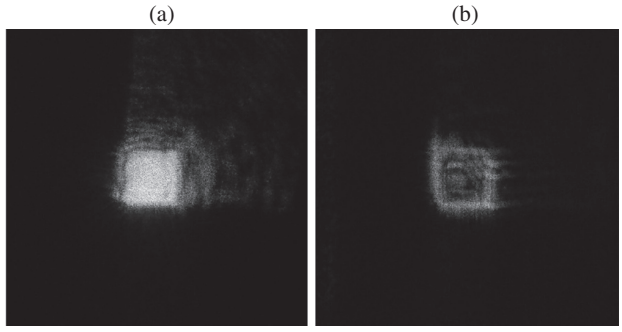

Fig. 5. Experimental Fourier processing of the image in the form of a square. (a) Image in the 0th order in the absence of signal at the AO filter and (b) image in the +1st order when the signal is applied to the AO filter.

In a strict consideration, events of not only anisotropic but also isotropic diffraction should be considered to describe the process of multiple diffraction in the geometry presented in Fig. 1. As shown in [8], the effectiveness of isotropic diffraction in TeO_2 is approximately only twice lower than the effectiveness of anisotropic diffraction. Basically, the radiation in our case will diffract not into three but into six diffraction orders and the diffraction process in this case should be described by a system of seven differential equations. Such a task can be solved only numerically. Notably, a process of diffraction in an intermediate region described by a system of 15 equations was investigated in [19], where the problem was solved numerically. In such an event, specific effects were discovered, such as the presence of three and five maxima in the 2nd and 3rd diffraction orders, respectively. However, these effects can be essentially referred to as the fine structure of AO interaction because they are observed only in the case of diffraction of plane waves and are strongly smoothened in the case of diverging optical and acoustic rays. In our case, all rays are definitely diverging. Therefore, we assumed that the consideration of higher diffraction orders would not significantly change the pattern of AO interaction in the intermediate region. Essentially, a simplified model was used when diffraction into only the three most effective orders was considered, yet it provided a qualitatively correct result. We believe

that the model describes the distribution of diffractive fields sufficiently well and demonstrates the presence of the areas that allow two-dimensional image processing, which is confirmed experimentally.

The obtained results significantly enhance the possibilities to apply AO elements in various devices. In particular, they can be used as two-dimensional spatial filters in image processing systems.

4. CONCLUSION

The following conclusions can be made based on the obtained results.

An AO spatial filter operating in an intermediate region of AO interaction was proposed for two-dimensional image processing. In comparison to the filters operating using the Bragg diffraction regime, the proposed filters operate at lower sound frequencies, which allows broadening of the band of the processed spatial frequencies and an increase in the limiting resolution of the image elements, thus allowing identification of smaller image features.

A simplified model based on the light diffraction into four orders including the 0th diffraction order was proposed to describe the filter operation. Transfer functions of the diffraction orders involved in the diffraction process were obtained based on the coupled-wave theory. The proposed model demonstrated a qualitatively correct result. It described the distribution of diffractive fields relatively well and demonstrated the presence of the areas that allow two-dimensional image processing. Based on this model, the transfer function of the first diffraction order allows the selection of a two-dimensional contour in the image in the course of its Fourier processing.

The obtained result was experimentally confirmed by optical Fourier processing of the image transmitted by the optical radiation at the wavelength of 0.63×10^{-4} cm. The AO cell of TeO_2 operating at the sound frequency of 15 MHz was used as a spatial filter. The length of AO interaction was 0.2 cm. The parameters of AO interaction corresponded to $Q = 2.07$.

Funding. Russian Foundation for Basic Research (19-07-00071).

REFERENCES

1. T. Y. Young and K.-S. Fu, *Handbook of Pattern Recognition and Image Processing* (Academic Press, Inc., New York, 1986).
2. H. Stark, *Applications of Optical Fourier Transforms* (Academic Press, New York, 1982).
3. A. A. Akaev and S. A. Maiorov, *Optical Methods for Data Processing* (Vysshaya Shkola, Moscow, 1988).
4. V. I. Balakshy and V. B. Voloshinov, "Acousto-optic image processing in coherent light," Quantum Electron. **35**(1), 85–90 (2005).
5. V. I. Balakshy, V. B. Voloshinov, T. M. Babkina, and D. E. Kostyuk, "Optical image processing by means of acousto-optic spatial filtration," J. Mod. Opt. **52**(1), 1–20 (2005).
6. V. B. Voloshinov, B. Linde, and K. B. Yushkov, "Improvement in performance of a TeO_2 acousto-optic imaging spectrometer," J. Opt. A: Pure Appl. Opt. **9**(4), 341–347 (2007).
7. V. I. Balakshy and D. E. Kostyuk, "Acousto-optic image processing," Appl. Opt. **48**(7), C24–C32 (2009).
8. V. I. Balakshy, V. N. Parygin, and L. E. Chirkov, *Physical Principles of Acousto-optics* (Radio i Svyaz', Moscow, 1985).
9. J. Xu and R. Stroud, *Acousto-optic Devices: Principles, Design and Applications* (Wiley, New York, 1992).
10. A. A. Yablokova, A. S. Machikhin, V. I. Batshev, V. E. Pozhar, and S. V. Boritko, "Analysis of transfer function dependence on configuration of acousto-optic interaction in uniaxial crystals," Proc. SPIE. **11032**, 1103215 (2019).
11. V. M. Kotov and S. V. Averin, "Two-dimensional image edge enhancement using two orders of Bragg diffraction," Quantum Electron. **50**(3), 305–308 (2020).
12. V. M. Kotov, G. N. Shkerdin, and S. V. Averin, "Formation of the two-dimensional image edge in two diffraction orders in the process of triple Bragg diffraction," J. Commun. Technol. Electron. **61**(11), 1090–1094 (2016).
13. V. M. Kotov, G. N. Shkerdin, and V. I. Grigor'evskii, "Polarization features of the 2D contouring of an optical image under double Bragg diffraction conditions," J. Commun. Technol. Electron. **58**(3), 226–232 (2013).
14. V. M. Kotov, S. V. Averin, and E. V. Kotov, "Selection of a two-dimensional image edge using polarisation-independent acousto-optic diffraction," Quantum Electron. **48**(6), 573–576 (2018).
15. V. M. Kotov, S. V. Averin, E. V. Kotov, and G. N. Shkerdin, "Acousto-optic filters based on the superposition of diffraction fields [Invited]," Appl. Opt. **57**(10), C83–C92 (2018).
16. V. M. Kotov, "Processing of 2D images using the Bragg diffraction," J. Commun. Technol. Electron. **65**(11), 1122–1127 (2020).
17. V. I. Balakshy, "Acousto-optical cell as a spatial filter," Radiotekh. Elektron. **29**(8), 1610–1616 (1984).
18. V. Yu. Rakovskii and A. S. Shcherbakov, "Multiphonon Bragg light scattering at the elastic waves," Zh. Tekh. Fiz. **60**(7) 107–114 (1990).
19. V. I. Balakshii and T. G. Kulish, "Higher orders of light diffraction by ultrasound in the intermediate regime of acoustooptical coupling," Opt. Spectrosc. **82**(4), 613–618 (1997) [Opt. Spektrosk. **82**(4), 663–668 (1997)].
20. V. I. Balakshy and T. G. Kulish, "High orders of light diffraction by ultrasound in the intermediate regime of acousto-optic interaction. I. Theoretical consideration," Acust. Acta Acust. **84**(5), 830–836 (1998).
21. V. I. Balakshy, I. V. Krylov, T. G. Kulish, and V. Y. Molchanov, "High orders of light diffraction by ultrasound in the intermediate regime of acousto-optic interaction. II. Experimental results," Acust. Acta Acust. **84**(5), 837–843 (1998).
22. R. Pieper, D. Koslover, and T.-C. Poon, "Exact solution for four-order acousto-optic Bragg diffraction with arbitrary initial conditions," Appl. Opt. **48**(7), C141–C150 (2009).
23. A. V. Zakharov, V. B. Voloshinov, and E. Blomme, "Intermediate and Bragg acousto-optic interaction in elastically anisotropic medium," Ultrasonics **51**(6), 745–751 (2011).
24. A. S. Shcherbakov and A. O. Arellanes, "Features of the three-phonon acousto-optical interaction due to elastic waves of finite amplitude and an advanced spectrum analysis of optical signals," J. Opt. Soc. Am. B **33**(9), 1852–1864 (2016).
25. V. M. Kotov, S. V. Averin, G. N. Shkerdin, and A. I. Voronko, "Two-dimensional image edge enhancement in the two-phonon diffraction," Quantum Electron. **40**(4), 368–370 (2010).
26. N. S. Piskunov, *Differential and Integral Calculus Volume 2* (Nauka, Moscow, 1970).
27. V. M. Kotov, "High-frequency two-color splitting of laser radiation," Opt. Spectrosc. **77**(3), 437–441 (1994) [Opt. Spektrosk. **77**(3), 493–497 (1994)].
28. M. P. Shaskol'skaya, *Acoustic Crystals* (Nauka, Moscow, 1982).
29. V. A. Kizel' and V. I. Burkov, *Crystal Gyrotropy* (Nauka, Moscow, 1980).